CAVITATION EVENT RATES AND NUCLEI DISTRIBUTIONS

Z. Liu, Y. Kuhn de Chizelle, and C. E. Brennen
California Institute of Technology
Pasadena, California

ABSTRACT

This paper examines the relationship between the cavitation event rates on axisymmetric headforms and the nuclei distributions in the incident flow. An analytical model is developed to relate these quantities and the results are compared with experimental cavitation event rates measured in the Large Cavitation Channel (LCC) at David Taylor Research Center (DTRC) on three different sizes of Schiebe body. The experiments were carried out at various cavitation numbers, tunnel velocities and air contents.

Boundary layer, bubble screening and observable cavitation bubble size effects on the event rates are examined. The trends in the event rates with changing cavitation number and body size are consistent with those observed experimentally. However the magnitudes of the event rates are about an order of magnitude larger than the experimental data. Nevertheless it is shown that the cavitation inception values predicted using a certain critical event rate are consistent with those observed experimentally.

Nomenclature

C	=Nuclei concentration
C_P	=Coefficient of pressure, $(p-p_\infty)/\frac{1}{2}\rho U^2$
C_{PM}	=Minimum C_P on a given streamline
C_{PMS}	=Minimum value of C_P on the headform surface
D	=Headform diameter
E	=Cavitation event rate
$N(R)$	=Nuclei density distribution function
R	=Radius of a cavitation nucleus
R_M	=Minimum radius of an observable cavitation bubble
R_C	=Critical cavitation nucleus radius
R_{max}	=Maximum cavitation bubble radius
S	=Surface tension
U	=Upstream tunnel velocity
U_M	=Maximum velocity corresponding to C_{PMS}
f_1, f_2, f_3	=Numerical factors effecting the cavitation event rate
p	=Fluid pressure
p_∞	=Pressure upstream
p_v	=Vapor pressure
r_H	=Headform radius
r_K	=Radius of curvature of streamlines near minimum pressure point
r_S	=Radius of minimum pressure point
r, y	=Normal distances of a given streamline from axis far upstream and from body surface near the minimum pressure point
s, s_0	=Coordinate along a streamline and the location of minimum pressure point
t_G	=Time available for bubble growth
u, u_M	=Fluid velocity, fluid velocity just outside boundary layer
v	=Velocity of a bubble normal to streamline
ρ	=Fluid density
σ	=Cavitation number, $(p_\infty-p_v)/\frac{1}{2}\rho U^2$
σ_{crt}	=Threshold cavitation number
σ_i	=Inception cavitation number
ξ, λ	=Factors in the chosen analytical expression for $N(R)$
ν	=Kinematic viscosity of fluid
μ	=Fluid viscosity
δ, δ_2	=Thickness and momentum thickness of boundary layer
ϵ	=Displacement of a bubble normal to streamline
Σ	=Function defined by equation (15).
Σ'	$=d\Sigma/d(r/r_H)$

1 Introduction

It has long been recognized that traveling bubble cavitation occurs as a result of micro-sized cavitation "nuclei" being convected into and then out of the low pressure regions in a flow. One consequence of this is the recognition that cavitation inception depends on the criterion one establishes in terms of the number of events per unit time. Because of the difficulties experienced in measuring the nu-

clei in a water tunnel (see Billet, 1985), there have been relatively few attempts to experimentally verify a relationship between the nuclei population in the incoming flow and the observed event rates. Two of the earliest attempts were the efforts by Ooi (1985) and Franklin and McMillan (1984) to synthesize the cavitation event rate in a submerged, turbulent jet (see also Pauchet *et al.*, 1992). However, one of the major uncertainties in that flow is the difficulty in characterizing the turbulent pressure fluctuations experienced by the bubble.

More recently Meyer *et al.* (1989,1992) have presented a theoretical model connecting the cavitation event rate on an axisymmetric headform with the nuclei distribution in the incident stream. The approximate analytical model presented by Ceccio and Brennen (1992) is similar in concept. The present paper refines this analytical model and adds the effects of the boundary layer, of bubble screening and of the finite size of the cavitation bubbles. Though more approximate than the numerical computations of Meyer *et al.* (1989, 1992), the analytical expressions provide insights into the important mechanisms and allow application in more complex flow geometries.

2 Experiments

The data presented in this paper was taken during tests conducted in the Large Cavitation Channel of the David Taylor Research Center in Memphis, Tennessee. Three geometrically similar axisymmetric headforms (Schiebe headform shape, Schiebe, 1972) measuring 5.08 cm, 25.4 cm and 50.8 cm in diameter were installed on the centerline of the tunnel and cavitation tests were conducted over a range of tunnel speeds (9 m/sec to 15 m/sec) and air contents (30% to 100% saturation at atmospheric pressure). The experimental arrangements are described elsewhere in greater detail (Kuhn de Chizelle *et al.*, 1992a,b) and will not be repeated here. It is sufficient to indicate that a large number of still photographs and a substantial quantity of video was taken for each operating condition (the video was synchronized to a strobe light to improve resolution).

Figure 1 presents the observed cavitation inception numbers, σ_i, as a function of headform diameter, D, tunnel velocity, U, and air-content relative to saturation at atmospheric pressure. Inception was based on an event rate of 50 cavitation events per second. Events were detected by means of flush-mounted electrodes, the current from which was modulated by the presence of a bubble (Ceccio and Brennen, 1992). The trends in figure 1 are fairly clear. The inception number increases with increasing headform size and the curves may well asymptote to the value of $(-C_{PMS})$. This headform size effect is simply a consequence of the fact that the larger the headform, the more nuclei are available for

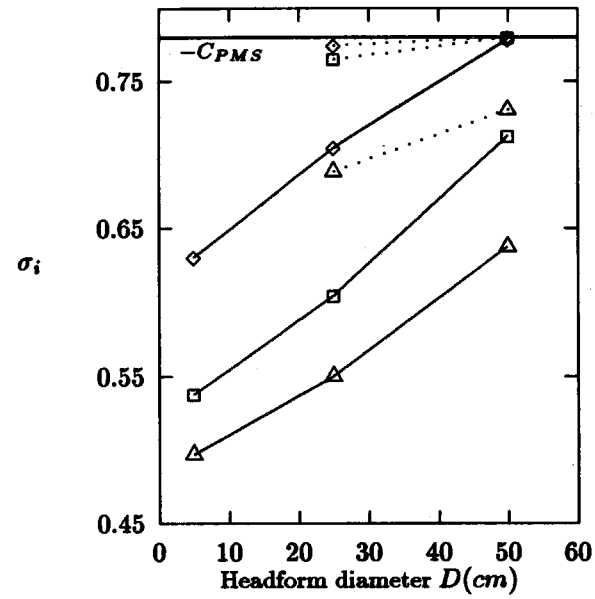

Figure 1: Experimentally observed cavitation inception numbers (based on 50 events/sec) as a function of tunnel velocity, headform size and air content. Velocity: 9 m/sec (◇), 11.5 m/sec (□) and 15 m/sec (△). Air content: 30% (——) and 80% (···)

cavitation and, therefore, for a specific event rate the value of σ_i will be larger. The values of σ_i also increase with increase in air content for a similar reason, namely more nuclei at the larger air contents. Figure 1 also demonstrates that the cavitation inception number increases with decreasing tunnel velocity. This effect is not so readily explained. However it is clear that to achieve the same cavitation number at a lower velocity one requires a higher tunnel pressure and it may be that the nuclei concentration in the tunnel increases considerably with decreasing operating pressure. We shall discuss this and other effects later in the paper.

3 Event Rate Observations

Both the photographs and the video tapes were analyzed in order to explore the variations in the cavitation event rates with headform size and tunnel velocity. The event rates were evaluated by counting the number of individual bubbles (or events) observable in a single frame and averaging this number over many frames. This allowed construction of figure 2 in which the average number of observable events is plotted against cavitation number, σ, for each of three velocities (9, 11.5 and 15 m/sec) for the three head-

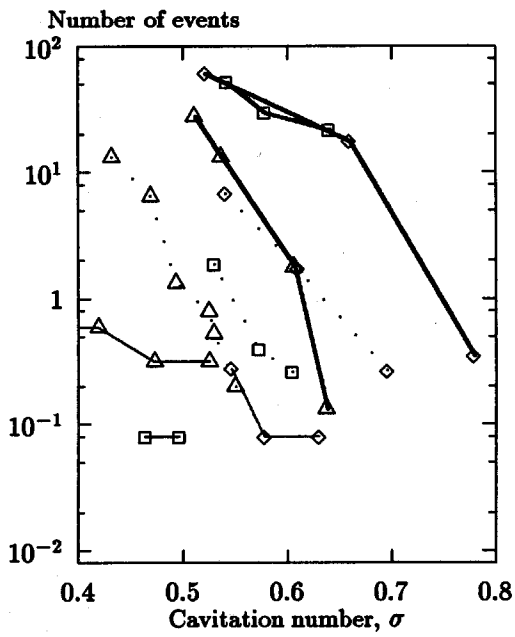

Figure 2: Average number of events observed on the headforms at an instant in time as a function of cavitation number, headform size and tunnel velocity. Velocity: 9 m/sec ($\diamond$), 11.5 m/sec ($\square$) and 15 m/sec ($\triangle$). Headform diameters: 5 cm (——), 25 cm (· · ·) and 50 cm (▬▬)

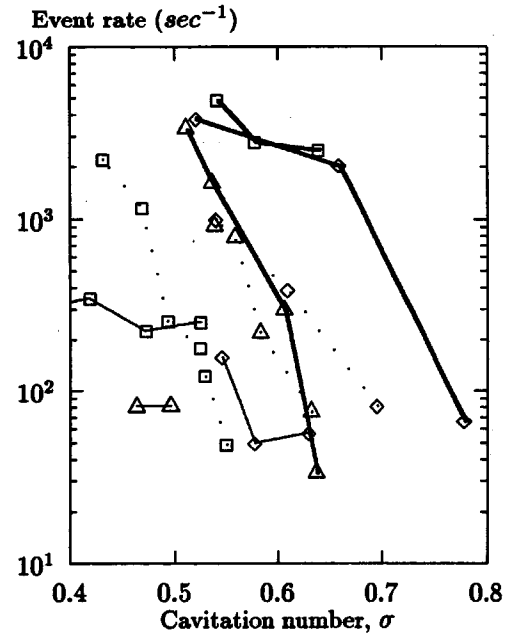

Figure 3: Cavitation event rates derived from figure 2 as a function of cavitation number, headform size and tunnel velocity. Velocity: 9 m/sec ($\diamond$), 11.5 m/sec ($\square$) and 15 m/sec ($\triangle$). Headform diameters: 5 cm (——), 25 cm (· · ·) and 50 cm (▬▬)

forms (this data is for 30% air content and we shall focus our attention on these conditions). Not surprisingly the number of events increases with decreasing cavitation number and with increasing headform size. Not so predictable is the tendency for the number of events to decrease with increasing speed but further comment on this effect is delayed until later.

The data on the number of events may be converted to cavitation event rates using bubble lifetimes obtained from knowledge of the velocity ($U_M = U(1 - C_{PMS})^{\frac{1}{2}}$ with C_{PMS} =-0.78) and the measured locations of bubble appearance and collapse as a function of σ (see Kuhn de Chizelle *et al.*, 1992a,b). The resulting event rate data for 30% air content is presented in figure 3 and it is clear that this is consistent with the cavitation inception data of figure 1 given the selected criterion of 50 events/sec.

As previously stated, one of the purposes of the present paper is to demonstrate the connection between the event rate (and by implication the inception number) and the nuclei number distribution. Before embarking on the details of this connection it is instructive to present the event rate data of figure 3 in the following modified form. Let us estimate that all the nuclei which pass through an annular stream tube bounded on the inside by the headform and on the outside by the stream surface which just touches the $C_P = -\sigma$ isobar (see figure 6) cavitate and therefore form observable bubbles. Then, using the potential flow velocity in this stream tube (therefore neglecting boundary layer effects) and using the data of figure 5 to estimate the thickness of the stream tube at each cavitation number, we can calculate the volume flow rate of liquid in the cavitating stream tube for each operating condition. Dividing the data of figure 3 by these values we obtain an estimate of the number of cavitation nuclei per unit liquid volume; this data is presented in figure 4. It is significant that some of the variation with cavitation number, headform size and tunnel velocity which was present in figures 2 and 3 has now been removed. Indeed, a large fraction of the data of figures 2 and 3 would appear to correspond to a nuclei concentration of the order of 0.1 nuclei/cm^3. The most noticeable deviation from this uniform value occurs at the highest speed (15 m/sec) with the two larger headforms.

The fact that a large fraction of the data appears to correspond to a similar nuclei concentration is simultaneously encouraging and puzzling. It is encouraging because it suggests that a more careful analysis which begins with the same nuclei number distribution and follows each nucleus along its streamline may allow synthesis of the event rates

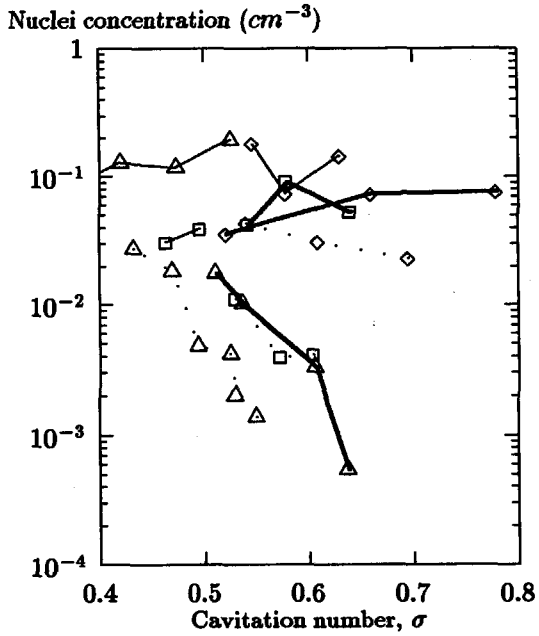

Figure 4: Effective concentrations derived from figure 3 as a function of cavitation number, headform size and tunnel velocity. Velocity: 9 m/sec (◇), 11.5 m/sec (□) and 15 m/sec (△). Headform diameters: 5 cm (——), 25 cm (···) and 50 cm (——)

and the inception numbers. But it is also puzzling because the concentration of 0.1 nuclei/cm^3 is at least an order of magnitude smaller than most of the measurements of cavitation nuclei would suggest.

Referring to Billet's (1985) useful review of the subject of nuclei concentrations and distributions we note that the most reliable observations of nuclei (microbubbles and particles) have been obtained by systematically surveying the reconstructed holograms of volumes of tunnel water taken while the tunnel is in operation (for example, Gates *et al.*, 1978, 1979). For de-aerated tunnel water, such inspections typically reveal concentrations more than 20 nuclei/cm^3 with sizes ranging from about 5μm to about 200μm (see also Kato, 1990). However the next question to ask is what fraction of these potential nuclei do, in fact, cavitate when subjected to sub-critical pressures. Here the answer is quite unclear. The other principal method for counting nuclei is the cavitation susceptibility meter in which the liquid is drawn through an orifice (or other device) and therefore is subjected to low pressures. The device is of sufficiently small size so that cavitation events occur individually. Then the concentration of potential cavitation nuclei (as opposed to potential nuclei) is obtained from the measured event rate and the known volume flow rate. Billet's review indicates that the typical concentrations measured by susceptibility meters are usually of the order of 2 nuclei/cm^3, significantly smaller than the concentrations obtained by holographic methods. While this may suggest that only a fraction of the potential nuclei actually cavitate, the data is, as yet, inadequate to support any firm conclusion and may, of course, differ significantly from facility to facility. However, insofar as the present experiments are concerned, it is clear that actual cavitation nuclei concentrations are normally much larger than 0.1 nuclei/cm^3. This suggests that some other mechanism comes into play to produce such a small event rate on the present headforms.

4 Analytical Model for Cavitation Event Rate

A simple synthesis of the cavitation event rate from the nuclei distribution in the on-coming stream was presented by Ceccio and Brennen (1992). Here we explore this relationship further and comment on other factors which could significantly effect the event rate. We will use a nuclei number distribution function, $N(R)$, defined such that, per unit volume, the number of nuclei with radii between R and $R + dR$ is given by $N(R)dR$. From the measurement of free stream nuclei distribution in our laboratory (see Liu *et al.*, 1993), a characteristic form for $N(R)$ is

$$N(R) = C\frac{\log e}{(2\pi)^{1/2}\lambda R} exp(-\frac{(\log R - \log \xi)^2}{2\lambda^2}) \qquad (1)$$

where C is the nuclei concentration. By adjusting the values of ξ and λ, the distribution function (1) can be made to fit most observed nuclei distribution functions. It is preferable to the more frequently used power law because it allows simulation of the peak in the population which is often observed (at $R = \xi$) and of the fact that the population of large bubbles is very small.

The problem is to evaluate how many of these nuclei are convected into the region of low pressure near the minimum pressure point on the surface of the body and therefore grow to observable macroscopic vapor bubbles. Some simplifying observations allow us to avoid lengthy numerical computations of the bubble dynamics (using the Rayleigh-Plesset equation) for every nucleus size, every streamline, every cavitation number, etc.. Meyer *et al.* (1989, 1992) conducted a detailed numerical study of this kind which included most of the effects studied here. In this paper we present a much simpler analytical approach which, though more approximate, is probably as accurate as the current experimental data would merit. Ceccio and Brennen (1992) observed while carrying out numerical integration of the Rayleigh-Plesset equation that, for a given cavitation number, σ, and minimum pressure coefficient, C_{PM}, all nuclei above a certain critical size, $R = R_C$, would grow to roughly the

same observable bubble size and therefore would be registered as "cavitation events". Furthermore, the critical size, R_C, appeared to be almost independent of the details of the pressure/time history and a function only of the difference between the minimum pressure and the vapor pressure (represented non-dimensionally by $(-C_{PM}-\sigma)$), the upstream velocity, U, the fluid density, ρ, and surface tension, S. Specifically,

$$R_C = \frac{8\beta S}{3\rho U^2(-C_{PM}-\sigma)} \qquad (2)$$

fitted the bubble dynamic calculations very well when the empirical parameter $\beta \approx 1$. This expression is, of course, consistent with the stability analyses put forward first by Flynn (1964) and Johnson and Hsieh (1966). Its use does save a great deal of computational effort. Furthermore, it means that we need not concern ourselves with the detailed pressure/time history along the entire length of each streamline but can simply focus on the region around the minimum pressure point.

However, it is necessary to determine how the minimum pressure coefficient, C_{PM}, varies from streamline to streamline. Here again we will use a simple analytic expression derived from much more complex computations. A panel method was developed to solve the potential flow around any axisymmetric headform. This was used to calculate the potential flow around the Schiebe headform. Such calculations suggested that the pressure gradient, dp/dy, normal to the surface in the vicinity of the minimum pressure point could be approximated by $\rho U_M^2/r_K$ where $U_M = U(1-C_{PMS})^{\frac{1}{2}}$ and C_{PMS} are respectively the velocity and pressure coefficient at the minimum pressure point on the surface of the body and r_K is a measure of the radius of curvature of the streamlines in this region. For the Schiebe body (C_{PMS} =-0.78) it is found that r_H/r_K =2.5 provides an approximate representation of the variation in the minimum pressure coefficient, C_{PM}, on a streamline with the distance y of that streamline from the surface. The actual variation of C_{PM} with y from the potential flow calculation is shown in figure 5 along with several approximations. With $dp/dy = \rho U_M^2/r_K$ it follows that

$$C_{PM} = C_{PMS} + 2y(1-C_{PMS})/r_K \qquad (3)$$

This expression allows us to evaluate from equation (2) the critical nuclei size, $R_C(y)$, for each streamline; R_C therefore increases with the distance, y, of the streamline from the surface. A larger critical size means that fewer of the available nuclei will generate cavitation events. The process is terminated on that streamline which just touches the isobar $C_{PM} = -\sigma$ for then the minimum pressure is equal to the vapor pressure and no cavitation events will occur on this streamline or any outside it. Consequently we need

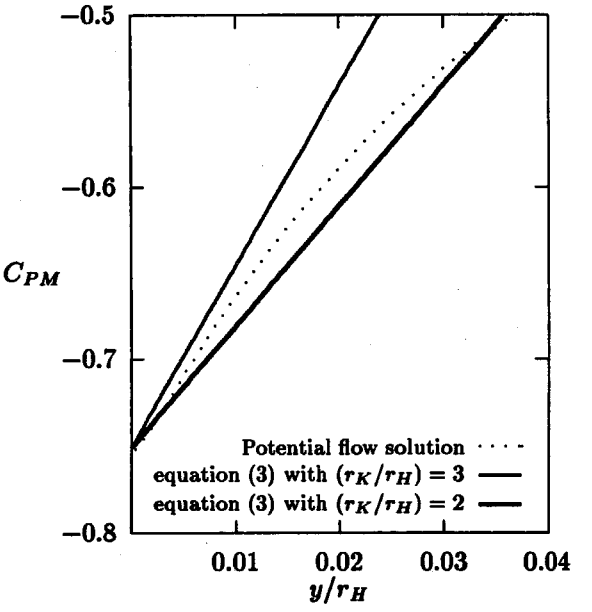

Figure 5: Variation in the minimum pressure coefficient, C_{PM}, on a streamline with the distance y of that streamline from the surface of the body near the minimum pressure point

only be concerned with a region near the surface given by

$$0 < y \leq y_M f_3 \qquad (4)$$

where

$$y_M = \frac{(-C_{PMS}-\sigma)}{2(1-C_{PMS})} r_K \qquad (5)$$

and f_3 =1. Different values of f_3 which is a function of R_M/r_H will be used later to examine the influence of a minimum observable bubble size, R_M. Using the relations (2) and (3) and disregarding any possible effects of the boundary layer or of relative motion between the nucleus and the flow one can then construct an event rate from the nuclei number distribution as follows. The volume flow rate passing through two stream surfaces a distance, dy, apart at the minimum pressure point (see figure 6) is given by

$$2\pi r_S U(1-C_{PMS})^{\frac{1}{2}} f_1(y)dy \qquad (6)$$

where $f_1(y)$ =1, but different values will be used later to account for boundary layer effects. The variable r_S is the radial distance from the axis of symmetry to the minimum pressure point (on the Schiebe body $r_S/r_H \approx 0.75$). It follows from equation (6) that the cavitation event rate in the stream tube, dE, is given by

$$dE = 2\pi r_S U(1-C_{PMS})^{\frac{1}{2}} f_1(y)dy \int_{R_C(y)}^{\infty} \frac{N(R)dR}{f_2(R,y)} \qquad (7)$$

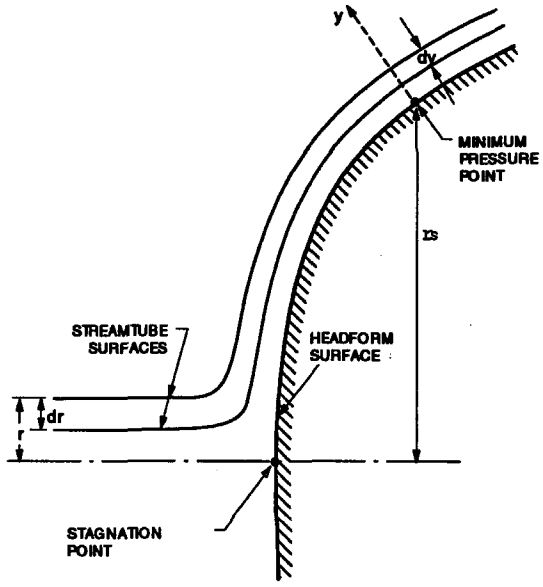

Figure 6: Schematic showing typical annular stream tube upstream and in the neighborhood of the minimum pressure point

where $f_2(R,y)$ =1, but different values will be used later to account for screening effects due to relative motion between the nuclei and the liquid. In the above equation it follows from equations (2) and (3) that

$$R_C(y) = \frac{8\beta S}{3\rho U^2}\left[-\sigma - C_{PMS} - \frac{2y(1-C_{PMS})}{r_K}\right]^{-1} \tag{8}$$

Note that $R_C(y \to y_M) \to \infty$. It follows that the total cavitation event rate, E, will be

$$E = \int_0^{y_M f_3} 2\pi r_S U(1-C_{PMS})^{\frac{1}{2}} f_1(y) \int_{R_C(y)}^{\infty} \frac{N(R)dR}{f_2(R,y)}dy \tag{9}$$

5 Boundary Layer Effect

The above analysis neglected the effects which the presence of a boundary layer might have on the pressure/time history experienced by a potential cavitation nucleus. Several such effects can be envisaged. These include the fact that the boundary layer will reduce the volume flow rate of fluid traveling close to the headform and thus reduce the supply of nuclei. It may also alter the shape of the isobars near the surface. Here we will explore only the first of these two effects. To do so we assume a simple form for the boundary layer profile near the minimum pressure point namely

$$\frac{u}{u_M} = \begin{cases} 2\left(\frac{y}{\delta}\right) - 2\left(\frac{y}{\delta}\right)^3 + \left(\frac{y}{\delta}\right)^4 & \text{for } y < \delta \\ 1 & \text{for } y \geq \delta \end{cases} \tag{10}$$

where δ is the boundary layer thickness. If δ_2 is the momentum thickness, it follows that $\delta_2 = 0.133\delta$ and using the modified Thwaites method to solve for the laminar boundary layer thickness (Thwaites, 1949, Rott and Crabtree, 1952), we find that

$$\frac{\delta_2}{r_H} \approx 0.68\left(\frac{\nu}{r_H U}\right)^{\frac{1}{2}} \tag{11}$$

Then, to account for the decrease in volume flow rate due to the boundary layer, the expressions (6), (7) and (9) should include non unity values for $f_1(y)$ given by

$$f_1(y) = \begin{cases} 2\left(\frac{y}{\delta}\right) - 2\left(\frac{y}{\delta}\right)^3 + \left(\frac{y}{\delta}\right)^4 & \text{for } y < \delta \\ 1 & \text{for } y > \delta \end{cases} \tag{12}$$

with $\delta = 5.10(\nu r_H/U)^{\frac{1}{2}}$.

It is also true that the boundary layer will effect the shape of the isobars and therefore cause some alteration of the expressions (3), (5), and (8); we have not included this effect in the present analysis.

6 Screening Effects

In their study of the potential cavitation of nuclei, Johnson and Hsieh (1966) recognized that the relative motion between the nuclei and the liquid might play an important role in determining the number of nuclei which enter the region in which the pressure is below the vapor pressure. Specifically they recognized that a bubble "screening" effect would occur in which the nuclei are forced away from the body due to the large pressure gradients normal to the streamlines in the vicinity of the stagnation point. This outward displacement would be larger for the larger bubbles. Because one is concerned only with streamlines very close to the stagnation streamline and the body surface and because the streamline curvature and therefore the pressure gradient normal to the streamline is much larger in the vicinity of the stagnation point than anywhere else, we may evaluate this screening effect by focusing attention on the stagnation point flow alone. In order to obtain an estimate of this effect we shall assume that the nuclei under consideration (of radius R) are all sufficiently small that the Reynolds number of the relative motion is much smaller than unity. Then the velocity of the nucleus in a direction normal to the streamline, v, is given by

$$v = \frac{2}{9}\frac{R^2}{\mu}\left(\frac{\partial p}{\partial n}\right) \tag{13}$$

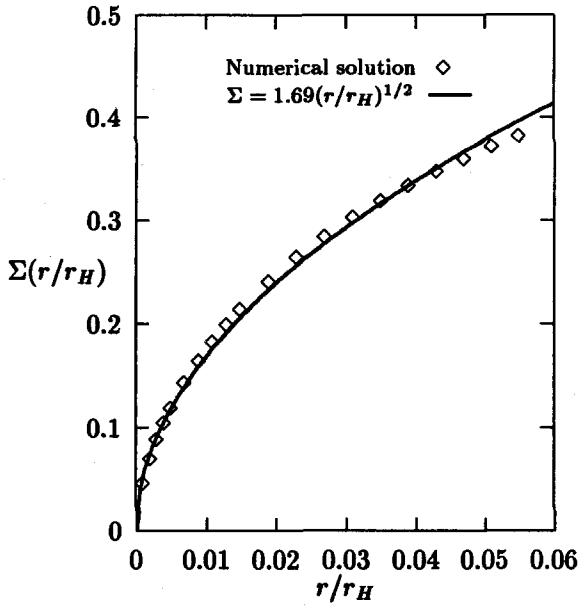

Figure 7: The function $\Sigma(r/r_H)$ for the stagnation point flow in the potential flow around a sphere

where $\partial p/\partial n$ is the local pressure gradient normal to the streamline. Then the total displacement, ϵ, across the streamlines is given by

$$\epsilon = \int_A^B v\, dt = \int_A^B \frac{v}{|q|} ds \tag{14}$$

where $|q|$ is the magnitude of the fluid velocity, the coordinate s is measured along a streamline, A is a point far upstream and B is a location after the large pressure gradients in the vicinity of the stagnation point have been experienced. Note that ϵ will, of course, differ from streamline to streamline and will therefore be a function of r defined as the radial position of the streamline far upstream of the body (see figure 6). Thus

$$\begin{aligned} \frac{\epsilon(r/r_H)}{r_H} &= \frac{2R^2U}{9\nu r_H}\int_A^B \frac{1}{\rho U^2}\frac{\partial p}{\partial(n/r_H)}\frac{U}{|q|}\, d(\frac{s}{r_H}) \\ &= \frac{2R^2U}{9\nu r_H}\,\Sigma(r/r_H) \end{aligned} \tag{15}$$

where $\Sigma(r/r_H)$ is used to denote the dimensionless integral on the previous line.

Since the stagnation point flow is the same on any blunt axisymmetric body it is appropriate to choose to examine the stagnation region in the potential flow around a sphere in order to evaluate $\Sigma(r/r_H)$. This is a non-trivial calculation, and the details will be omitted here for the sake of brevity. The result is the function $\Sigma(r/r_H)$ presented in figure 7; for convenience this can be approximated by the empirical relation

$$\Sigma(r/r_H) = \Gamma(r/r_H)^\gamma \tag{16}$$

where $\Gamma \approx 1.69$, $\gamma \approx 0.5$.

Having evaluated the screening displacement it can be applied to the evaluation of the event rate in the following way. A nucleus of radius R which is on the streamline at radius r far upstream will, when it reaches the low pressure region, be on the streamline which is the following distance, y, from the body surface:

$$\frac{y}{r_H} = \frac{1}{2(1-C_{PMS})^{\frac{1}{2}}}\frac{r^2}{r_S r_H} + \frac{2}{9}(\frac{R}{r_H})^2\frac{r_H U}{\nu}\Sigma(r/r_H) \tag{17}$$

Thus the stream tube between y and $y+dy$ will contain all the nuclei of radius R which were present in the upstream flow between radii r and $r+dr$ (figure 6) where

$$\frac{dy}{r_H} = \frac{r\, dr}{(1-C_{PMS})^{\frac{1}{2}} r_S r_H} f_2(R,y) \tag{18}$$

and

$$f_2(R,y) = 1 + \frac{2}{9}(\frac{R}{r_H})^2(\frac{r_H U}{\nu})(1-C_{PMS})^{\frac{1}{2}}(\frac{r_S}{r_H})\frac{r_H}{r}\Sigma' \tag{19}$$

where Σ' denotes $d\Sigma/d(r/r_H)$ and r and y are related by equation (17). Since the liquid flow between y and $y+dy$ is still given by the expression (6), it follows that the actual number distribution function for the stream tube between y and $y+dy$ is $N_E(R,y)$ where

$$N_E(R,y) = N(R)/f_2(R,y) \tag{20}$$

Consequently the screening effect alters the event rate by introducing a non-unity expression for $f_2(R,y)$ in the expression (9), namely that given by equation (19).

7 Observable cavitation bubble size effect

Normally, experimental observation can only detect cavitating bubbles when they achieve a certain observable size, say R_M, and in this section we shall incorporate this "observable cavitation bubble size effect" in our analysis. This requires an analysis of the maximum size, R_{max}, achieved by the cavitation bubble. To do so we represent the pressure coefficient near the minimum pressure point approximately by

$$\begin{aligned} C_P &= C_{PMS} + \frac{2y(1-C_{PMS})}{r_K} + \frac{C^*_{P1}|s-s_0|}{r_H} \\ &= C_{PM} + \frac{C^*_{P1}|s-s_0|}{r_H} \end{aligned} \tag{21}$$

where s is a coordinate measured along a streamline and s_0 is the minimum pressure location. C_{PM} is given by equation (3). The value of the constant C^*_{P1} is about 1.39. It follows that the time of residence of the bubble in the region $-C_P \leq \sigma$ on a given streamline distance y from the surface is given by

$$t_G = \frac{2(-\sigma - C_{PM})}{UC^*_{P1}(1 - C_{PMS})^{1/2}} r_H \tag{22}$$

The bubble growth rate is given approximately by

$$\frac{dR}{dt} = U(-\sigma - C_{PM})^{1/2} \tag{23}$$

where C_{PM} is given by equation (3). It follows that the maximum size, R_{max}, a cavitating bubble can reach will be given roughly by

$$\frac{R_{max}}{r_H} = \frac{2(-\sigma - C_{PM})^{3/2}}{C^*_{P1}(1 - C_{PMS})^{1/2}} \tag{24}$$

Only those bubbles whose maximum size, R_{max}, is greater than a certain radius, R_M, are regarded as observable cavitation events. By solving $R_{max} \geq R_M$ for y, we have

$$y \leq y_M f_3(R_M/r_H) \tag{25}$$

where

$$f_3(\frac{R_M}{r_H}) = 1 - \frac{\left[\frac{1}{2}\left(\frac{R_M}{r_H}\right) C^*_{P1}(1 - C_{PMS})^{1/2}\right]^{2/3}}{(-\sigma - C_{PMS})} \tag{26}$$

and y_M is given by (5). Notice that as $R_M \rightarrow 0$, $f_3(R_M/r_H) \rightarrow 1$. And when

$$\sigma_{crt} = -C_{PMS} - \left[\frac{1}{2}(\frac{R_M}{r_H}) C^*_{P1}(1 - C_{PMS})^{1/2}\right]^{2/3} \tag{27}$$

$f_3(R_M/r_H) = 0.$, which means that if $\sigma \geq \sigma_{crt}$, there will be no bubbles with sizes greater than R_M. Hence σ_{crt} is the threshold cavitation number. For example, for C_{PMS} =-0.78 and R_M/r_H =0.04, σ_{crt} is 0.67, which is far less than $-C_{PMS}$ =0.78.

8 Results of Analytical Model

In this section we shall evaluate the various effects on the cavitation event rate and compare the results of the analytical model with the measured cavitation event rates of figure 3 and the inception data of figure 1. For this purpose we select a particular nuclei number distribution of the form given by equation (1), namely

$$\begin{aligned} C &= 100 cm^{-3} \\ \xi &= 13.0\,\mu m \\ \lambda &= 0.43 \end{aligned} \tag{28}$$

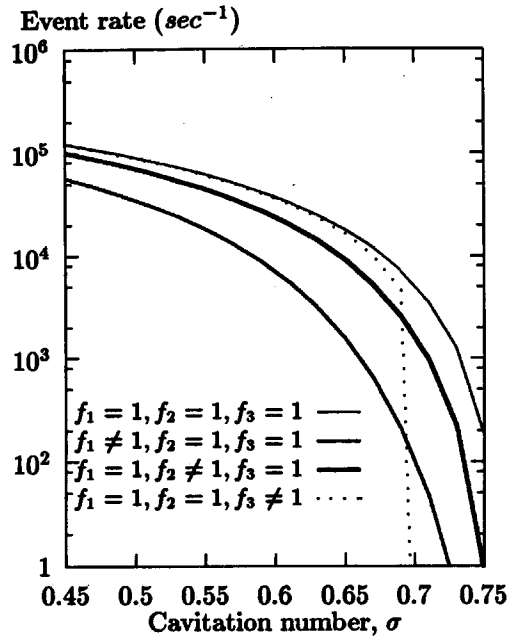

Figure 8: Example of the effects of boundary layer volume flow (f_1), bubble screening (f_2) and observable cavitation bubble size (f_3) on the calculated event rates. D =5cm, U =9 m/sec, R_M =1.0mm

These values produce a shape which is similar to that of many of the nuclei number distributions which have been measured in our laboratory (Liu *et al.*, 1993). We note that the concentration, C, of 100 cm^{-3} is consistant with the measurement done by other researchers. It is much larger than that proposed by Billet (1985), but is less than those measured by Gates (1978) and Kato (1990). When viewing the analytical results in figures 8 and 9, one should remember that the cavitation event rates simply scale linearly with concentration C and therefore the results for other values of concentration C are easily obtained.

In figure 8, we present typical results showing the characteristic effects of boundary layer volume flow (f_1), of the bubble screening (f_2) and of the observable cavitation bubble size (f_3). Note that all these effects can cause a significant reduction in the event rate and, together, can account for an order of magnitude reduction in the event rate. Among all the effects, the boundary layer flow rate effect causes the biggest reduction in the event rate. Also note that the observable cavitation bubble size restriction sets up a sharp threshold at cavitation number of about 0.69. However, from figure 9, even with these effects taken into account, the event rates are still about an order of magnitude larger than observed experimentally.

The event rates predicted by equation (9) with $f_1 \neq 1$,

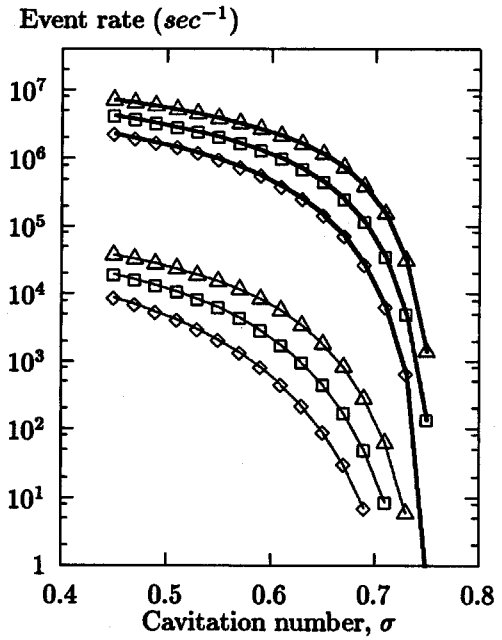

Figure 9: Calculated cavitation event rates for the 5 cm (——), and 50 cm (▬▬) headforms at 9 m/sec (◇), 11.5 m/sec (□) and 15 m/sec (△). Boundary layer volume flow and the bubble screening effects are included. The observable cavitation bubble size effect is not included

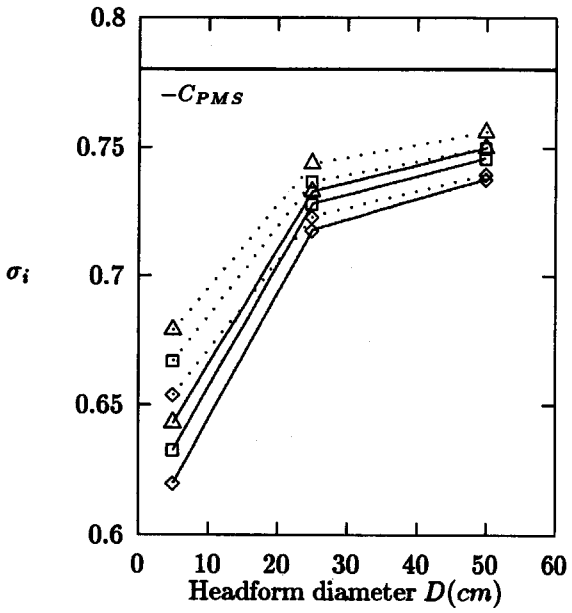

Figure 10: Predicted cavitation inception numbers for various tunnel velocities (9 m/sec (◇), 11.5 m/sec (□), and 15 m/sec (△)), headform diameters and two minimum observable bubble sizes of R_M =1 mm (——) and R_M =0.5 mm (···)

$f_2 \neq 1$, $f_3 = 1$ are shown in figure 9. Note that the variations in the event rates with cavitation number and with headform size are qualitatively similar to the experimental trends in figure 3. But there are also two substantial discrepancies. First the tunnel velocity effect produced by the model is not consistent with that observed experimentally, having a different sign in the experiments. Secondly, the magnitude of the event rate is at least one order of magnitude larger than that observed experimentally.

We must conclude that two outstanding issues still remain. First the observed event rates are at least one order of magnitude smaller than one would predict based on the anticipated nuclei distributions. Perhaps only a small fraction of the "potential" nuclei actually do cavitate but more detailed study is needed to confirm this. Secondly the changes with tunnel velocity cannot be explained at present. One suspects that the observed effects may be the result of changes in the nuclei population with changes in the tunnel operating condition (pressure and velocity). On-line monitoring of nuclei content and explorations of how the nuclei content changes with operating condition seem essential prerequisites for answering the questions posed by this study. Moreover, it seems clear that cavitation inception criteria are a natural consequence of the event rate variations and that the above recommendations are also an essential prerequisite to an understanding of inception and the scaling effects of cavitation.

The information on event rates can be used to produce cavitation inception numbers simply by selecting a certain event rate criterion for inception. Notice in figure 8 that the observable cavitation bubble size effect has the largest influence at large cavitation numbers.

The cavitation inception numbers will mostly depend on the the ratio of R_M/r_H. For example, when R_M/r_H =0.04 or 0.004, the cavitation inception number can not exceed the threshold cavitation number σ_{crt} which has a value of 0.67 or 0.75 respectively. The fact that this effect does not show up in the experimental data in figure 1 is probably because of the counteracting effects of the tunnel blockage on the large headforms in the LCC. For example, when the overall tunnel cavitation number was 0.78, the blockage effect on the 50.8 cm headform would create an effective value of 0.70 in the low pressure region.

In the work of Ceccio and Brennen (1992), the minimum detectable cavitation bubble radius on 5 cm diameter Schiebe bodies was about 1 mm. Figure 10 shows the predicted cavitation inception numbers for various body sizes and various velocities with R_M =1.0 mm and R_M =0.5

mm. Comparing figure 10 with figure 1, the trends of predicted cavitation inception numbers with changing headform sizes are consistent with the experimental observations. And the values are also close to those experimentally observed.

9 Conclusion

The present paper consists of an intermediate report on an investigation of the relationship between cavitation nuclei distributions in a water tunnel and the cavitation event rates on some axisymmetric headforms. Data on the event rate for a series of headforms of different size installed in the DTRC Large Cavitation Channel is presented and analyzed. It is shown that the event rate scales with size and speed in a manner which is consistent with a simple model and a fairly constant nuclei concentration. Cavitation inception numbers based on a fixed event rate also seem to scale as expected with headform size and, crudely, with air content. However the scaling with speed seems the opposite of that which one would expect based on a constant nuclei concentration and suggests that the concentration changes substantial with tunnel pressure and speed.

A simple analytical model is presented for the connection between the nuclei distribution and event rate. Similar in concept to the numerical model presented by Meyer *et al.* (1989, 1992), it has the advantage of ease of calculation and adaptation to other flows. The effects of the reduction in volume flow due to the boundary layer, of the bubble screening near the stagnation point and of a minimum observable cavitation bubble size are included. Combined these effects give rise to a reduction in the event rate of an order of magnitude.

Comparison of the experiments with the model using a constant nuclei distribution characteristic of those measured in our laboratory reveals two important discrepancies. The event rates observed in the LCC experiments are fairly consistently about one order of magnitude less than expected. This may be due to the fact that only a small fraction of the observed nuclei actually cavitate or it may be due to some other effect which is not included in the model. The other discrepancy has already be mentioned, namely that the trend with velocity is the reverse of that observed experimentally. As mentioned above, this could well be due to a nuclei distribution which changes substantially with tunnel operating conditions. Experiments in our laboratory show that the nuclei distribution can change in this way (Liu *et al.*, 1993).

When the model for the event rates is used with some chosen criterion to predict the cavitation inception number, the results are consistent with those observed experimentally in so far as the trend with headform size is concerned. The trend with velocity is, of course, at odds with the experiments because of the same discrepancy in the event rate.

Acknowledgements

The authors are very grateful to Professor S. L. Ceccio for the major role he played in the experimental observations. The help of Douglas Hart, Young Shen, Scott Gowing and James Blanton is also gratefully acknowledged. This work was supported by the Office of Naval Research under contract number N-00014-91-K-1295.

References

Billet, M. L., 1985, "Cavitation Nuclei Measurement – A Review," *ASME Cavitation and Multiphase Flow Forum Booklet*, pp. 31-38.

Ceccio, S. L. and Brennen, C. E., 1992, "Observations of the dynamics and acoustics of traveling bubble cavitation," *J. Fluid Mech.*, Vol. 233, pp. 633-660

Flynn, H. G., 1964, "Physics of Acoustic Cavitation in Liquids. *Physical Acoustics: Principles and Methods*, 16ed. (W. P. Mason), pp. 57-172., Academic Press.

Franklin, R. E. and McMillan, J., 1984, "Noise Generation in Cavitating Flows, the Submerged Jet," *ASME J. Fluids Eng.*, Vol. 106, pp. 336–341.

Gates, E. M. and Bacon, J., 1978, "A Note on the Determination of Cavitation Nuclei Distributions by Holography," J. of Ship Research, Vol. 22, No. 1, pp. 29-31.

Gates, E. M., Billet, M. L., Katz, J., Ooi, K. K., Holl, W. and Acosta, A. J., 1979, "Cavitation Inception and Nuclei Distribution – Joint ARL-CIT Experiments," *Rep. E244-1.* California Institute of Technology, Division of Engineering and Applied Science.

Johnson, V. E. and Hsieh, T., 1966, "The Influence of Gas Nuclei on Cavitation Inception," *Proc. Sixth Symposium on Naval Hydrodynamics, Washington, D.C.*, National Academy Press.

Kato, H., 1990, "Cavitation," Maki Press, Tokyo, Japan, pp. 20-23.

Kuhn De Chizelle, Y., Ceccio, S. L., Brennen C. E. and Shen, Y., 1992a, "Cavitation Scaling Experiments with Headforms: Bubble Dynamics," *Proc. Second International Symposium on Propeller and Cavitation*, Hangzhou, China.

Kuhn De Chizelle, Y., Ceccio, S. L., Brennen C. E. and Shen, Y., 1992b, "Cavitation Scaling Experiments with Headforms: Bubble Acoustics," *Proc. Nineteenth Symposium on Naval Hydrodynamics*, Seoul, Korea.

Lindgren, H. and Johnsson, C. A., 1966, "Cavitation Inception on Headforms: I.T.T.C. Comparative Experiments," *Proc. Eleventh Intl. Towing Tank Conference, Tokyo.*

Liu, Z., Sato, K. and Brennen, C. E., 1993, "Cavitation Nuclei Population Dynamics in a Water Tunnel," *ASME Cavitation and Multiphase Flow Forum*, Washington, D.C..

Meyer, R. S., Billet, M. L. and Holl, J. W., 1989, "Free Stream Nuclei and Cavitation," *Intl. Symposium on Cavitation Inception, ASME FED* , pp. 55-62.

Meyer, R. S., Billet, M. L. and Holl, J.W., 1992, "Free stream Nuclei and Traveling Bubble Cavitation," *ASME J. Fluids Eng.*, Vol. 114, pp. 672-679.

Ooi, K. K., 1985, "Scale Effects on Cavitation Inception in Submerged Water Jets: A New Look," *J. Fluid Mech.*, Vol. 151, pp. 367–390.

Pauchet, J., Retailleau, A. and Woillez, J., 1992, "The Prediction of Cavitation Inception in Turbulent Water Jets," *ASME Cavitation and Multiphase Flow Forum Booklet*, FED, Vol. 135, pp. 149–158.

Rott, N. and Crabtree, L. F., 1952, "Simplified Laminar Boundary Layer Calculations for Bodies of Revolution and for Yawed Wings," *J. Aero. Sci.*, Vol. 19, pp. 553-565.

Schiebe, F. R., 1972, "Measurement of the Cavitation Susceptibility of Water Using Standard Bodies," *Rep. 118*, St. Anthony Falls Hydraulic Labl, University of Minnesota.

Thwaites, B., 1949, "Approximate Calculation of the Laminar Boundary Layer," *Aero. Quart.*, Vol. 1, pp. 245-280.